Soluble Narrow-Band-Gap Copolymers Containing Novel Cyclopentadithiophene Units for Organic Photovoltaic Cell Applications

KUANG-CHIEH LI,[1] YING-CHAN HSU,[2] JIANN-T'SUEN LIN,[2] CHANG-CHUNG YANG,[3] KUNG-HWA WEI,[1] HONG-CHEU LIN[1]

[1]Department of Materials Science and Engineering, National Chiao Tung University, Hsinchu, Taiwan, Republic of China

[2]Institute of Chemistry, Academia Sinica, Taipei, Taiwan, Republic of China

[3]Energy and Environmental Laboratories, Industrial Technology Research Institute, Hsinchu, Taiwan, Republic of China

ABSTRACT: Five novel conjugated copolymers (**P1**–**P5**) containing coplanar cyclopentadithiophene (CPDT) units (incorporated with arylcyanovinyl and keto groups in different molar ratios) were synthesized and developed for the applications of polymer solar cells (PSCs). Polymers **P1**–**P5** covered broad absorption ranges from UV to near infrared (400–900 nm) with narrow optical band gaps of 1.38–1.70 eV, which are compatible with the maximum solar photon reflux. Partially reversible p- and n-doping processes of **P1**–**P5** in electrochemical experiments were observed, and the proper molecular design for highest occupied molecular orbital (HOMO)/lowest unoccupied molecular orbital (LUMO) levels of **P1**–**P5** induced the highest photovoltaic open-circuit voltage in the PSC devices, compared with those previously reported CPDT-based narrow-band-gap polymers. Powder X-ray diffraction (XRD) analyses suggested that these copolymers formed self-assembled π-π stacking and pseudobilayered structures. Under 100 mW/cm^2 of AM 1.5 white-light illumination, bulk heterojunction PSC devices containing an active layer of electron donor polymers **P1**–**P5** mixed with electron acceptor [6,6]-phenyl C$_{61}$ butyric acid methyl ester (PCBM) in the weight ratio of 1:4 were investigated. The PSC device containing **P1** gave the best preliminary result with an open-circuit voltage of 0.84 V, a short-circuit current of 2.36 mA/cm^2, and a fill factor of 0.38, offering an overall power conversion efficiency (PCE) of 0.77% as well as a maximal quantum efficiency of 23% from the external quantum efficiency (EQE) measurements. © 2009 Wiley Periodicals, Inc. J Polym Sci Part A: Polym Chem 47: 2073–2092, 2009

Keywords: conjugated polymers; copolymerization; cyclopentadithiophene; heteroatom-containing polymers; polymer solar cell

INTRODUCTION

The developments of new materials to be used in organic optoelectronic devices such as polymeric solar cells (PSCs) have become dramatically

attractive because they represent a green and renewable energy alternative to fossil energy and nuclear power. In particular, the so-called bulk heterojunction (BHJ) concept[1] has been established in thin films of organic solar cell devices utilizing electron-donating conjugated polymers blended with electron-accepting species, such as fullerenes,[2(a)] dicyano-based polymers,[2(b,c)] or *n*-type nanoparticles.[3] For these purposes, several novel polymeric materials have been extensively studied over the past decade. For example, the regio-regular poly(3-hexylthiophene) (P3HT)[4] and poly[2-methoxy-5-(3′,7′-dimethyloctyloxy)-*p*-phenylenevinylene] (MDMO-PPV)[5] possessed a highest power conversion efficiency (PCE) approaching 5.0% in PSCs. However, several groups proposed new polymeric structures as substitutes for these polymers, since the disadvantages on the PSC performance were somehow restricted by their relatively large band gaps,[6] which only absorbed part of the visible light and limited the utility of the sunlight.

To further improve the absorption properties of the conjugated polymers, the intramolecular charge transfer (ICT) interactions between electron-donor (D) and electron-acceptor (A) moieties have been extensively applied to the developments of novel narrow-band-gap conjugated polymers with better PSC performance, especially in the band-gap region of 1.4–1.8 eV.[7–16] Among them, the derivatives of polyfluorene,[7] thiophene-based,[8] and arylamine-based[9] represent promising features having PCE values. However, besides band gaps, several characteristics of conjugated polymers, including highest occupied molecular orbital (HOMO)/lowest unoccupied molecular orbital (LUMO) levels and carrier mobilities, need to be simultaneously optimized to achieve higher photovoltaic performance.[10]

Recently, to obtain longer conjugation lengths, more planar molecular geometries, and more rigid structures in π-conjugated polymers,[11(a)] novel heteroaromatic fused-ring derivatives, including cyclopentadithiophene (CPDT) units, have been widely investigated in PSCs. Kraak et al. first reported the structural unit of CPDT in 1968,[12(a)] and the later prepared CPDT-based polymers[12(b,c),13] showed relatively high conductivities due to more extensive π-conjugation lengths as compared with polythiophene and polyfluorene derivatives. Because of the high planarities, long conjugation lengths, narrow band gaps, and strong intermolecular π-π interactions of the CPDT units, CPDT-based polymers possessing

good conductive properties were found to be a powerful approach to optimize the PSC performance. Recently, the derivatives of CPDT copolymers showed very promising PCE results (1.14–5.5%)[14] and high carrier mobilities (10^{-2}–10^{-1} cm^2/Vs),[14(c),15] which demonstrated that the synthesized ICT polymers possess both prominent properties of narrow band gaps and high carrier mobilities.

Up to now, very few investigations of CPDT-based polymers have been reported for the applications of PSC performance. Although the band gaps of the reported derivatives of CPDT homopolymers and copolymers were relatively low,[11–16] their HOMO energy levels were apparently not low enough to produce air-stable polymers with relatively high open circuit potential (V_{oc}) values in the ultimate PSC devices, where the highest V_{oc} values of the CPDT-based polymers were still not over 0.65 V.[14,15] It is noticeable that a well-known design to tune the HOMO and LUMO levels of conjugated polymers would be the introduction of electron-withdrawing units, such as nitro, carboxy, and cyano groups, to the conjugated systems.[17] In 1991, Ferraris and Lambert reported that CPDT-based polymers, bearing electron-withdrawing keto groups at the bridging carbons, showed relatively low band gap values around 1.20 eV.[16(a)] On the other hand, another important observation was found that the electron-withdrawing cyano groups could decrease the HOMO level and thus to stabilize the neutral state of the conjugated system.[17(a)]

On the basis of this concept, two different moieties of CPDT derivatives, that is, 2,6-diarylene-cyanovinylene-CPDT (**M1**) and CPDT-4-one (**M2**), were utilized as acceptor monomers to synthesize CPDT-based copolymers **P1**–**P5**. Besides, to increase the solubility without causing any additional twisting of the repeating units in the resulting copolymers, 4-carbon position of compound **2** could be favorably functionalized by diethylhexyl substitutions to produce CPDT unit (**3**) as the donor monomer. Therefore, our donor-acceptor approaches utilized in these CPDT-based copolymers (**P1**–**P5**) achieve the absorption spectra in the visible range of 400–850 nm (with tailing up to around 1000 nm) in solid films and finely tuned HOMO and LUMO levels with narrow electrochemical band gaps of 1.30–1.66 eV. In addition, after thermal annealing, the molecular configurations of the π-conjugated CPDT-based copolymers could clearly ensure that highly organized π-π stackings could be easily formed in these fused-

heteroaromatic molecular frameworks, which were confirmed by the powder X-ray diffraction (XRD) analyses. Compared with those reported CPDT-based polymers, our copolymers in this report showed much improved V_{oc} values with a highest open-circuit voltage up to 0.84 V as well as suitable electronic energy levels and good processabilities for PSC applications. So far, the preliminary PSC performance of these structurally related copolymers showed the best PCE efficiency up to 0.77% while blended with [6,6]-phenyl C_{61} butyric acid methyl ester (PCBM), with a short circuit current density (I_{sc}) of 2.36 mA/cm^2, an open circuit voltage (V_{oc}) of 0.84 V, and a fill factor (FF) of 0.38 under AM 1.5 (100 mW/cm^2). Although the results for the PCE efficiencies of these un-optimized PSCs are not sufficiently high enough, this research affords a new concept to enhance the V_{oc} properties via the electron donor-acceptor (D-A) design to offset the low V_{oc} drawbacks, which are generally encountered in narrow-band-gap CPDT-based conjugated polymers.

EXPERIMENTAL

Materials

All chemicals and solvents were used as received. Compounds **1** (cyclopenta[2,1-b:3,4-b']dithiophen-4-one)[18] and **2** (4H-cyclopenta [2,1-b:3,4-b']dithiophene)[13(c)] were synthesized according to the literature procedures. The synthetic routes of monomers **1**–**2** and polymers **P1**–**P5** are shown in Schemes 1 and 2, and the synthetic procedures of their intermediates were described. Chemicals and solvents were reagent grades and purchased from Aldrich, ACROS, TCI, and Lancaster Chemical. Toluene, tetrahydrofuran, and diethyl ether were distilled to keep anhydrous before use.

Measurements and Characterization

^{1}H NMR spectra were recorded on a Varian Unity 300 MHz spectrometer using CDCl$_3$ solvents. Elemental analyses were performed on a HERAEUS CHN-OS RAPID elemental analyzer. Transition temperatures were determined by differential scanning calorimetry (DSC; Perkin-Elmer Pyris 7) with a heating and cooling rate of 10 °C/min. Thermogravimetric analyses (TGA) were conducted with a TA instrument Q500 at a heating rate of 20 °C/min under nitrogen. Gel permeation chromatography (GPC) analyses were conducted on a Waters 1515 separation module using poly-
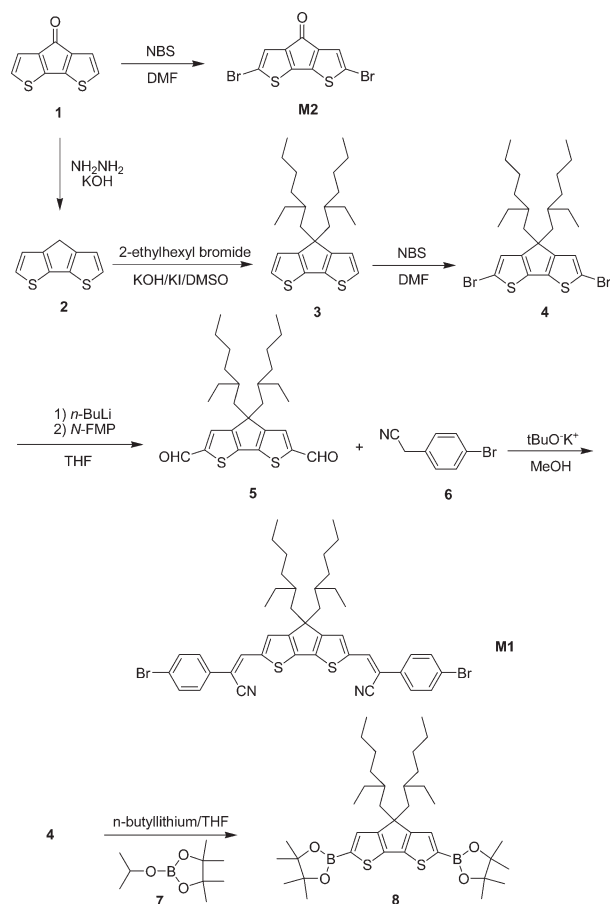
Scheme 1. Synthetic routes of monomers **1**, **2**.

styrene as a standard and THF as an eluent. UV-visible absorption and photoluminescence (PL) spectra were recorded in dilute chloroform solutions (10^{-6} M) on a HP G1103A and Hitachi F-4500 spectrophotometer, respectively. Solid films of UV-vis and PL measurements were spin-coated on a quartz substrate from chlorobenzene solutions with a concentration of 10 mg/mL. Cyclic voltammetry (CV) measurements were performed using a BAS 100 electrochemical analyzer with a standard three-electrode electrochemical cell in a 0.1 M tetrabutylammonium hexafluorophosphate (TBAPF6) solution (in acetonitrile) at room temperature with a scanning rate of 50 mV/s. In each case, a carbon working electrode coated with a thin layer of these copolymers, a platinum wire as the counter electrode, and a silver wire as the quasi-reference electrode were used. Ag/AgCl (3 M KCl) electrode was served as a reference electrode for all potentials quoted herein. During the CV measurements, the solutions were purged with nitrogen for 30 s, and the redox couple ferrocene/ferrocenium ion (Fc/Fc$^+$) was used as an
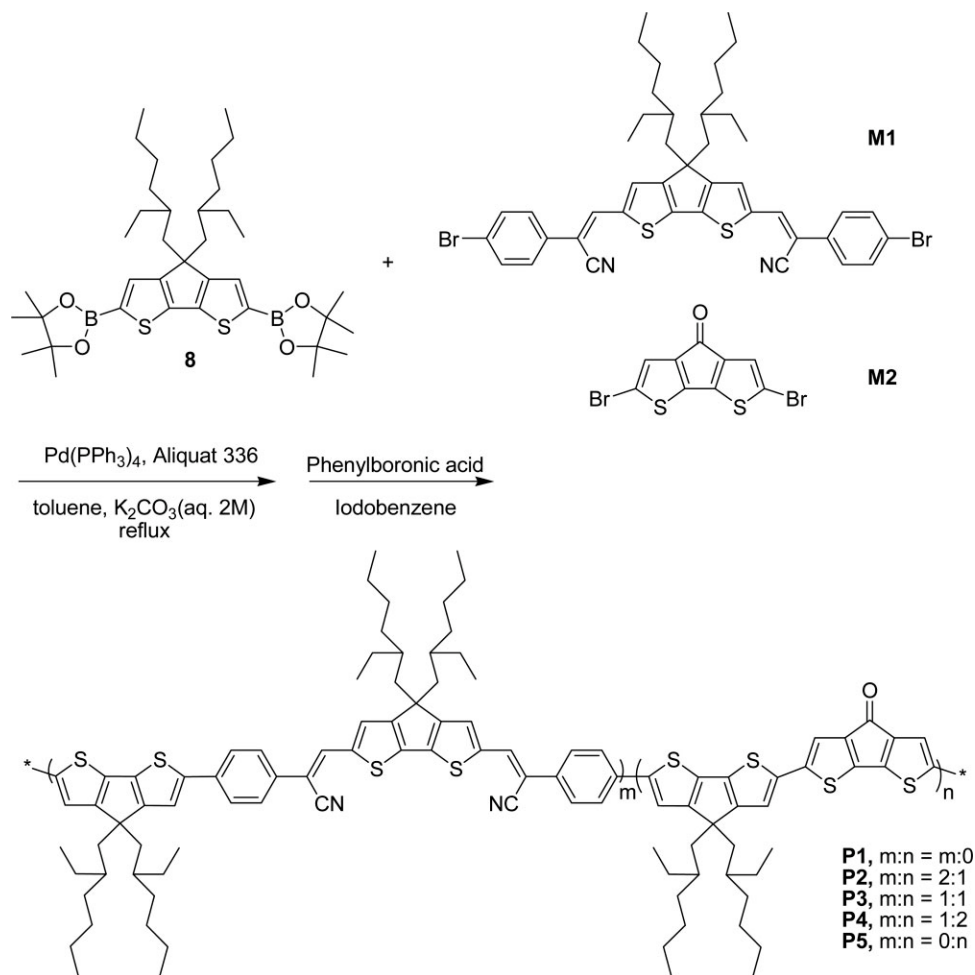
Scheme 2. Synthetic routes of copolymers **P1**–**P5**.

external standard. The corresponding HOMO and LUMO levels in copolymer films of **P1**–**P5** were calculated from $E_{ox/onset}$ and $E_{red/onset}$ values of the electrochemical experiments. The LUMO value of PCBM was in accordance with the literature data.[19(b)] Each onset potential in the CV measurements was defined by the intersection of two tangents drawn at the rising current and background current.

X-Ray Diffraction Characterization

Synchrotron powder XRD measurements were performed at beamline BL17A of the National Synchrotron Radiation Research Center (NSRRC), Taiwan, where the wavelength of X-ray was 1.33361 Å. The XRD data were collected using Mar345 image plate detector mounted orthogonal to the beam with sample-to-detector distance of 250 mm, and the diffraction signals were accumulated for 3 min. The powder samples were packed into a capillary tube and heated by a heat gun, whose temperature controller is programmable by a PC with a PID feedback system. The scattering angle θ was calibrated by a mixture of silver behenate and silicon.

Fabrication of Hole- and Electron-Only Devices

The hole- and electron-only devices in this study containing copolymers **P1**–**P5**: PCBM (1:4) blend film sandwiched between transparent ITO anode and cathode. The ITO glasses were first ultrasonically cleaned in detergent, de-ionized water, acetone, and isopropyl alcohol before the deposition. After routine solvent cleaning, the substrates were treated with UV ozone for 3 min. In the hole-only device, the modified ITO surface was obtained by spin-coating a layer of poly (ethylene dioxythiophene): polystyrenesulfonate (PEDOT:PSS) (~50 nm). After baking at 100 °C for 1 h, the substrates were then transferred into

a nitrogen-filled glove box. The active layer was spin coated (spin rate = 500 rpm; spin time = 40 s) on top of PEDOT:PSS and then dried in covered glass Petri dishes. The film thicknesses of the active layer were measured to be 370, 320, 260, 420, and 290 nm for **P1, P2, P3, P4**, and **P5**, respectively. Subsequently, a 15 and 120 nm thick of MoO_3 and aluminum was thermally evaporated under vacuum at a pressure below 2.5×10^{-5} torr through a shadow mask. The active area of the device was 0.0314 cm^2. In the electron-only device, the PEDOT:PSS layer was replaced with Cs_2CO_3, which has been used as an efficient electron injection layer. The modified ITO surface was obtained by spin-coating a layer of Cs_2CO_3 (∼2 nm). The film thicknesses of the active layer were measured to be 340, 240, 280, 260, and 460 nm for **P1**, **P2**, **P3**, **P4**, and **P5**, respectively. Subsequently, a 40 and 70 nm thick of Ca and aluminum was thermally evaporated under vacuum at a pressure below 2.5×10^{-5} torr through a shadow mask. The active area of the device was 0.0314 cm^2.

Device Fabrication and Characterization of Polymer Solar Cells

The photovoltaic cell (PVC) device structure used in this study was a sandwich configuration of ITO/PEDOT:PSS/active layer/LiF/Al, where the active layer was made of electron donor polymers **P1–P5** mixed with electron acceptor [6,6]-phenyl C_{61} butyric acid methyl ester (PCBM) in the weight ratio of 1:4 (w/w). The PVC devices were fabricated according to the procedures similar to those of EL devices. An ITO-coated glass substrate was precleaned and treated with oxygen plasma before use. A thin layer (∼50 nm) of PEDOT:PSS was spin-coated on an ITO substrate and heated at 130 °C for 1 h. Subsequently, the preliminary active layer was prepared by spin coating from composite solutions of **P1–P5**/PCBM (1:4 w/w) in chlorobenzene (10 mg/mL) on the top of the PEDOT:PSS layer. The spin rate was about 800 rpm, and the thickness of the active layer was typically ranged between 100 and 160 nm, unless the detailed thickness is specified. The PVC devices were completed by deposition with 1 nm of LiF and 120 nm of Al. The film thicknesses were measured by a profilometer (Dektak3, Veeco/ Sloan Instruments). For PVC measurements, *I–V* curves were recorded under a solar simulator with AM 1.5 irradiation (at 100 mW/cm²). A 300 W xenon lamp (Oriel, #6258) with AM 1.5 filter

(Oriel, #81,080 kit) was used as the white light source, and the optical power at the sample was 100 mW/cm² detected by Oriel thermopile 71,964. The *I–V* characteristics were measured using a CHI 650B potentiostat/galvanostat. The external quantum efficiency (EQE) was measured using a CHI 650B coupled with Oriel Cornerstone 260 monochromator. All PVC devices were prepared and measured under ambient conditions.

Synthesis

4,4-Bis(2-ethylhexyl)-4H-cyclopenta[2,1-b:3,4-b′]dithiophene (3)

Compound **2** (2.0 g, 11.2 mmol) was dissolved in DMSO (50 mL), and then 2-ethylhexyl bromide (4.3 g, 22.4 mmol) was added and followed by potassium iodide (50 mg). The mixture was purged with nitrogen and cooled in an ice bath, and ground KOH (2.0 g) was added in portions. The resulting green mixture was vigorously stirred overnight at room temperature. Water was added after reaction, and the reaction mixture was extracted with dichloromethane. Consequently, the organic layer was separated and dried with magnesium sulfate. Solvent was removed under vacuum, and the crude product was purified by chromatography using hexane as eluent. Subsequently, the pure compound was obtained as colorless oil. Yield: 3.60 g (80%).

^{1}H NMR (ppm, $CDCl_3$): δ 7.13 (m, 2H), 6.91 (m, 2H), 1.86 (m, 4H), 0.93 (m, 18H), 0.73 (t, J = 6.4 Hz, 6H), 0.59 (m, J = 7.2 Hz, 6H).

2,6-Dibromo-4,4-bis(2-ethylhexyl)-4H-cyclopenta[2,1-b:3,4-b′]dithiophene (4)

Compound **3** (3.5 g, 8.7 mmol) and NBS (3.1 g, 17.4 mmol) were dissolved in 50 mL of DMF. The resulting solution was stirred to react at room temperature under nitrogen overnight. Water (50 mL) was then added and the organic phase was extracted with dichloromethane (100 mL) twice, washed with water, and dried with magnesium sulfate. After that, the solvent was removed under reduced pressure to obtain the product. The crude product was purified by column chromatography with hexane to obtain pale yellow oil (4.10 g). Yield: 83%.

^{1}H NMR (ppm, $CDCl_3$): δ 6.92 (s, 2H), 1.80 (m, 4H), 0.94 (m, 18H), 0.76 (m, 6H), 0.60 (m, J = 7.2 Hz, 6H).

4,4-Bis(2-ethylhexyl)-4H-cyclopenta[2,1-b:3,4-b′]dithiophene-2,6-dicarbaldehyde (5)

To a solution of compound **4** (4.4 g, 7.8 mmol) in THF (80 mL), *n*-BuLi (2.5 M solution in hexane, 7.0 mL, 17.9 mmol) was added at −78 °C. After stirring for 1 h, a solution of *N*-formylmorpholine (1.9 g, 16.4 mmol) in THF (20 mL) was added. After an additional stirring for 1 h at −78 °C, the mixture was allowed to warm up to room temperature. Next, the mixture was hydrolyzed by 1 N HCl, and the final solution was extracted with dichloromethane. The organic layer was dried over magnesium sulfate and the solvent was evaporated. Afterward, the crude product was purified by column chromatography (silica gel, EA/hexane 1:10) to yield a yellow solid. Yield: 83%.

^{1}H NMR (ppm, CDCl$_3$): δ 9.88 (s, 2H), 7.61 (s, 2H), 1.94 (m, 4H), 0.96–0.86 (m, 18H), 0.71 (m, 6H), 0.55 (m, J = 7.2 Hz, 6H).

2,6-Bis(4,4,5,5-tetramethyl-1,3,2-dioxaborolan-2-yl)-4,4-Bis(2-ethylhexyl)-4H-cyclopenta[2,1-b:3,4-b′]dithiophene (8)

A solution of compound **4** (6.5 g, 11.6 mmol) in 150 mL of dry THF was stirred in a two-necked flask and cooled at −78 °C while *n*-butyllithium (2.5 M solution in hexane, 29.0 mmol) was added dropwise under nitrogen atmosphere. After reaction for 2 h at −78 °C, compound **7** (6.0 mL, 29.0 mmol) was added carefully to the mixture solution at −78 °C and then the mixture was allowed to warm up to react at room temperature overnight. The final solution was acidified with 100 mL of 10% HCl solution and stirred for 45 min at room temperature. The solution was extracted by dichloromethane and the organic layer was dried over magnesium sulfate. After removing the solvent by rotavapor, the crude product was purified by column chromatography (silica gel, CH$_2$Cl$_2$/hexane 1:2) to afford compound **8** (4.93 g). Yield: 65%.

^{1}H NMR (ppm, CDCl$_3$): δ 7.43 (s, 2H), 1.84 (m, 4H), 1.35 (m, 24H), 0.95–0.56 (m, 30H). ^{13}C NMR (ppm, CDCl$_3$): δ 160.95 (2C), 144.06 (2C), 131.86 (2C), 126.34 (2C), 83.89 (4C), 52.64 (2C), 43.17, 35.11 (2C), 33.84 (2C), 28.30 (2C), 27.42 (2C), 24.74 (8C), 22.75 (2C), 14.06 (2C), 10.55 (2C). MS (FAB): *m/z* [M$^+$] 655; calcd *m/z* [M$^+$] 654.4. Anal. calcd for C$_{37}$H$_{60}$B$_2$O$_4$S$_2$: C, 67.89; H, 9.24; S, 9.80. Found: C, 67.92; H, 9.52; S, 10.29.

M1

A mixture of compound **5** (2.6 g, 5.6 mmol), compound **6** (i.e., 1-bromophenylacetonitrile, 5.5 g, 28 mmol), and methanol (300 mL) were mixed in a 500 mL two-neck round-bottom flask at room temperature. A catalytic amount of potassium *tert*-butoxide in methanol was added into this mixture. After reaction for 24 h, the product was filtered and dried. Chromatography on silica gel eluted with CH$_2$Cl$_2$/hexane 1:4 afforded **M1** as a red solid (4.1 g). Yield: 90%.

^{1}H NMR (ppm, CDCl$_3$): δ 7.62–7.48 (m, 12H), 1.95 (m, 4H), 0.97–0.90 (m, 16H), 0.75–0.59 (m, 14H). ^{13}C NMR (ppm, CDCl$_3$): δ 160.42 (2C), 140.25 (2C), 134.38 (2C), 134.25 (2C), 133.02 (2C), 132.25 (4C), 126.93 (4C), 126.67 (2C), 122.87 (2C), 118.23 (2C), 105.34 (2C), 54.21 (2C), 43.07, 35.29 (2C), 34.09 (2C), 28.43 (2C), 27.30 (2C), 22.73 (2C), 14.01 (2C), 10.62 (2C). MS (FAB): *m/z* [M$^+$] 815; calcd *m/z* [M$^+$] 814.1. Anal. Calcd for C$_{43}$H$_{46}$Br$_2$N$_2$S$_2$: C, 63.39; H, 5.69; N, 3.44; S, 7.87. Found: C, 63.58; H, 5.39; N, 3.55; S, 8.22.

2,6-Dibromocyclopenta[2,1-b:3,4-b′]dithiophen-4-one (M2)

The synthesis of compound **M2** was also followed by the similar procedure of compound **4**. Compound **1** (2.0 g, 10.4 mmol) was dissolved in 50 mL of dimethylformamide under nitrogen in the dark, and NBS (3.8 g, 20.8 mmol) was added gradually. The crude product was purified by column chromatography with CH$_2$Cl$_2$/hexane (1:1) to get a purple solid (3.1 g). Yield: 85%.

^{1}H NMR (ppm, CDCl$_3$): δ 6.98 (s, 2H). ^{13}C NMR (ppm, CDCl$_3$): δ 182.56, 150.07 (2C), 143.54 (2C), 124.41 (2C), 113.95 (2C). MS (EI): *m/z* [M$^+$] 350; calcd *m/z* [M$^+$] 349.8. Anal. Calcd for C$_9$H$_2$Br$_2$OS$_2$: C, 30.88; H, 0.58; S, 18.32. Found: C, 31.10; H, 0.71; S, 18.42.

General Procedure for the Syntheses of Copolymers P1–P5

The synthetic routes of polymers are shown in Scheme 2.[20] All of the polymerization procedures were carried out through the palladium(0)-catalyzed Suzuki coupling reactions. In a 50 mL two-neck flask, 1 equiv of dibromo compounds (**M1** and **M2** with various molar ratios, **M1**:**M2** = *m*:0, 2:1, 1:1, 1:2, and 0:*n*, respectively) and 1 equiv of 2,6-bis(4,4,5,5-tetramethyl-1,3,2-dioxaborolan-2-yl)-4,4-Bis(2-ethylhexyl)-4H-cyclopenta[2,1-b:3,4-

b′]dithiophene (**8**) were added into 10 mL of anhydrous toluene. The Pd(0) complex, tetrakis(triphenylphosphine)palladium (1 mol %), was transferred into the mixture in a dry environment. Then, 2 M aqueous potassium carbonate and a phase transfer catalyst, that is, aliquat 336 (several drops), were subsequently transferred via dropping funnel the previous mixture under nitrogen. The reaction mixture was stirred at 85 °C for 2 days and then both excess amounts of iodobenzene and phenylboronic acid, the end-cappers, dissolved in 1 mL of anhydrous toluene were added and stirred for 4 h, respectively. The reaction mixture was cooled to 50 °C and added slowly into a vigorously stirred mixture of methanol/water (10:1). The polymers were collected by filtration and reprecipitation from methanol. The crude polymers were further purified by washing with acetone for 3 days in a Soxhlet apparatus to remove oligomers and catalyst residues. The chloroform fractions (350–400 mL) were reduced to 40–50 mL under reduced pressure and were precipitated in acetone and finally air-dried overnight.

P1

Following the general polymerization procedure, compound **8** (1.0 equiv) and **M1** (1.0 equiv) were used in this polymerization to acquire a black powder. Yield: 50%.

^{1}H NMR (ppm, CDCl$_3$): δ 7.67 (br, m, 14H), 1.99 (br, m, 8H), 1.02–0.67 (br, m, ~60H). Elem. Anal. Calcd: C, 77.37; H, 7.83; N, 2.65; S, 12.15. Anal. Found: C, 77.89; H, 7.35; N, 2.77; S, 12.17.

P2

Following the general polymerization procedure, compound **8** (1.0 equiv), **M1** (0.67 equiv), and **M2** (0.33 equiv) were used in this polymerization to attain a black powder. Yield: 80%.

^{1}H NMR (ppm, CDCl$_3$): δ 7.67 (broad), 7.05 (s), 1.98 (broad), 1.02–0.68 (broad). Elem. Anal. Found: C, 74.97; H, 7.06; N, 2.65; S, 13.87; O, 0.96.

P3

Following the general polymerization procedure, compound **8** (1.0 equiv), **M1** (0.5 equiv), and **M2** (0.5 equiv) were used in this polymerization to obtain a black powder. Yield: 67%.

^{1}H NMR (ppm, CDCl$_3$): δ 7.65 (broad), 7.04 (s), 1.96 (broad), 1.00–0.66 (broad). Elem. Anal.

Found: C, 73.43; H, 6.97; N, 2.33; S, 15.01; O, 1.53.

P4

Following the general polymerization procedure, compound **8** (1.0 equiv), **M1** (0.33 equiv), and **M2** (0.67 equiv) were used in this polymerization to gain a black powder. Yield: 81%.

^{1}H NMR (ppm, CDCl$_3$): δ 7.66 (broad), 7.02 (s), 1.96 (broad), 1.25–0.69 (broad). Elem. Anal. Found: C, 72.13; H, 7.59; N, 1.67; S, 16.30; O, 1.79.

P5

Following the general polymerization procedure, compound **8** (1.0 equiv) and **M2** (1.0 equiv) were used in this polymerization to get a black powder. Yield: 56%.

^{1}H NMR (ppm, CDCl$_3$): δ 7.01 (br, s, 4H), 1.93 (br, m, 4H), 1.25–0.67 (br, m, ~30H). Elem. Anal. Calcd: C, 69.11; H, 6.48; S, 21.70; O, 2.71. Anal. Found: C, 69.73; H, 6.09; S, 21.04; O, 3.18.

RESULTS AND DISCUSSION

Syntheses and Chemical Characterization

As outlined in Scheme 1, two electron-accepting monomers **M1** and **M2** based on CPDT moieties were prepared from cyclopenta[2,1-b:3,4-*b*′]dithiophen-4-one (**1**)[18] using a reduction procedure and followed by dibromination, which were described by Turner and coworkers.[13(c)] The electron-donating unit of CPDT (**8**) was prepared by dilithiation of **4** with *n*-buthyllithium and followed by reaction with compound **7** to afford 4,4-dialkyl-2,6-bis(4,4,5,5-tetramethyl-1,3,2-dioxaborolan-2-yl)-4*H*-cyclopenta[2,1-*b*:3,4-*b*′]dithiophene **8** (see Scheme 1). Monomers **M1**–**M2** and compound **8** were satisfactorily characterized by ^{1}H NMR, ^{13}C NMR, MS spectroscopies, and elemental analyses. Three-component random copolymers **P2**–**P4** were prepared successfully via Suzuki coupling of compound **8** with a mixture of various molar ratios of monomers **M1** and **M2**. Two-component copolymers **P1** and **P5** were produced by compound **8** copolymerized with monomers **M1** and **M2**, respectively. The synthetic procedures toward copolymers **P1**–**P5** are outlined in Scheme 2. Most copolymers are partly soluble in organic solvents such as chloroform, THF, and chlorobenzene at room temperature and

Table 1. Molecular Weights, Yields, and Thermal Data of Polymers 1–5

Polymer	Feeding Ratio (m:n)	Output Ratio (m:n)[a]	M_n[b]	M_w[b]	PDI	Yield (%)	T_m[c] (°C)	T_d[d] (°C)
P1	m:0	m:0	15000	28800	1.92	50	n.d[e]	388
P2	2:1	1.58:1	22900	60800	2.65	80	229	360
P3	1:1	0.87:1	14500	26300	1.81	67	192	355
P4	1:2	1:1.87	10200	17400	1.71	81	200	320
P5	0:n	0:n	6900	9700	1.41	56	200	311

[a] Output molar ratios of m:n in copolymers **P2**–**P4** were calculated from the elemental analyses.
[b] Molecular weights (M_n: number average molecular weight; M_w: weight average molecular weight) and PDI values were measured by GPC, using THF as an eluent, polystyrene as a standard.
[c] Melting transition temperatures (°C) were measured by DSC at a heating rate of 10 °C/min.
[d] Decomposition temperatures (°C) at 5% weight loss (T_d) were measured by TGA at a heating rate of 20 °C/min under nitrogen.
[e] No noticeable T_m was observed.

completely soluble in high boiling point solvents (e.g., chlorobenzene) at high temperature. The yields and molecular weights of polymers **P1**–**P5** determined by GPC against polystyrene standards in THF are summarized in Table 1. These results show that considerable molecular weights with high yields (50–81% after Soxhlet extractions) were obtained in these copolymers, where the weight-average molecular weights (M_w) ranging 9700–60,800 with polydispersity indices (PDI $= M_w/M_n$) of 1.41–2.65 were obtained.

The molecular structures of copolymers **P1**–**P5** were identified by ^{1}H NMR and FT-IR. The output ratios of copolymers **P2**–**P4** were calculated from the elemental analyses, which are all reasonably close to the feeding ratios of copolymers **P2**–**P4**. Proton NMR spectra of monomers **M1**–**M2** and copolymers **P1**–**P5** in CDCl$_3$ are illustrated in Figure 1. The characteristic resonances at 7.67 and 7.01 ppm in the spectra of **P1**–**P5** are assigned to two different protons of monomers **M1** and **M2**, respectively. In addition, the peak area ratios of output copolymers between the two resonances at 7.67 ppm (**M1**) and 7.01 ppm (**M2**) in the NMR spectra fitted well with the designed molecular structures of copolymers **P1**–**P5**, where a larger integrated signal of $\delta = 7.01$ ppm could be observed in the copolymers with a higher molar ratio of **M2**. The molecular structures of polymers **P1**–**P5** could also be confirmed by the FT-IR spectra. For instance, the absorption stretching mode of the cyano group in the copolymers, which typically appears at 2210/cm, was absent in the spectrum of copolymer **P5**, and the intensity of this band decreased as the molar ratio of **M1** unit reduced from **P1** to **P4**. In contrast, a characteristic band at 1710/cm for C=O stretching was observed in these copolymers, which was absent in the spectrum of copolymer **P1**, and the intensity of this band increased as the molar ratio of **M2** unit increased from **P2** to **P5**.

The thermal stabilities and phase transition properties of copolymers **P1**–**P5** were characterized by TGA and DSC measurements under nitrogen atmosphere, and the thermal decomposition temperatures (T_d) and melting points (T_m) are summarized in Table 1. It is apparent that all copolymers exhibited good thermal stabilities, which showed less than 5% weight loss upon heating to 311–388 °C. Regarding DSC experiments, there were no distinct glass transition temperatures (T_g) for all copolymers. Except for **P1**, these copolymers showed relatively sharp transitions appearing around 192–229 °C, which were attributed to the melting of the polymer backbones. The absence of sharp transition in **P1** was probably originated from four 2-ethylhexyl irregular side chains belonging to monomers **8** and **M1**.

Optical Properties

The optical absorption spectra of D-A copolymers **P1**–**P5** in chloroform solutions (10^{-6} M) and solid films are shown in Figure 2, and their photophysical properties are demonstrated in Table 2. As can be seen, the absorption energy band gaps of CPDT-based copolymers **P1**–**P5** could be finely tuned by the molar ratios of electron-accepting units **M1** and **M2** (**M1**:**M2** $= m$:0, 2:1, 1:1, 1:2, and 0:n), and their absorption spectra covered broad wavelength ranges for both solutions and solid films. The longer maximum absorption wavelengths of **P1** (584 nm) and **P5** (705 nm) in chloroform solutions of Figure 2(a) were about 88 nm and 192 nm red-shifted from the corresponding absorption wavelength of monomers **M1** (496
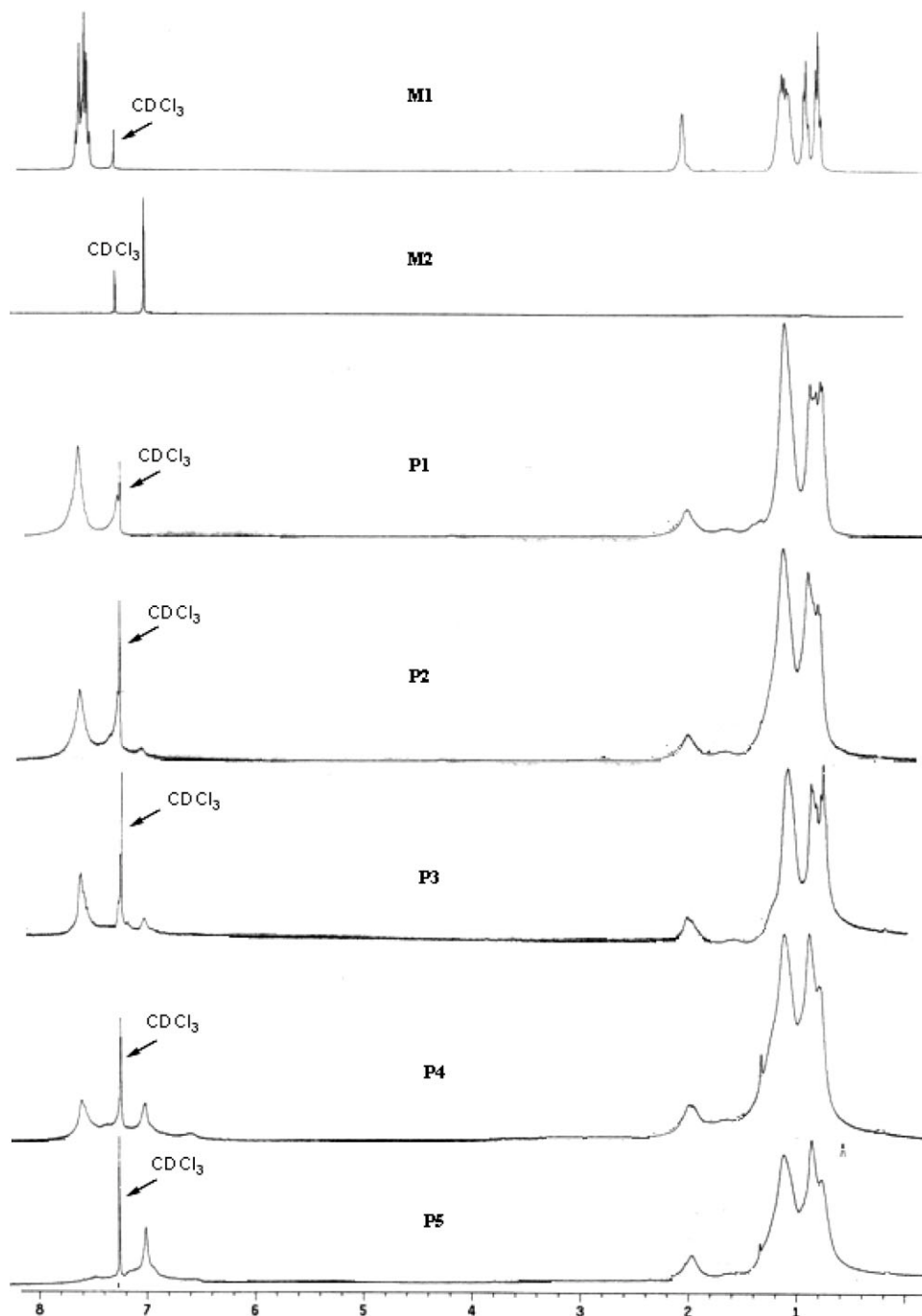
Figure 1. ^{1}H NMR spectra of monomers **M1**, **M2** and polymers **P1–P5** in CDCl$_3$.

nm) and **M2** (513 nm), respectively, reflecting much longer effective conjugation lengths of the extended coplanar CPDT-based polymer backbones. However, it is noted that **P1** exhibited one maximum absorption wavelength λ_{max} at 584 nm, which was significantly longer (and had a longer conjugation length) than that of the related homopolymer poly(4,4-dialkyl-4H-cyclopenta[2,1-b:3,4-

b']dithiophen) (**PCPDT** with λ_{max} = 565 nm and alkyl = 2-ethylhexyl).[13(b)] Similar trends of UV-vis spectra were observed in rigid conjugated polymers with strong ICT interactions between electron donor and acceptor moieties.[21] Surprisingly, the UV-vis spectrum of **P5** displayed two well-separated peaks at 484 nm and 705 nm, which were originated from two individual UV-vis absorption
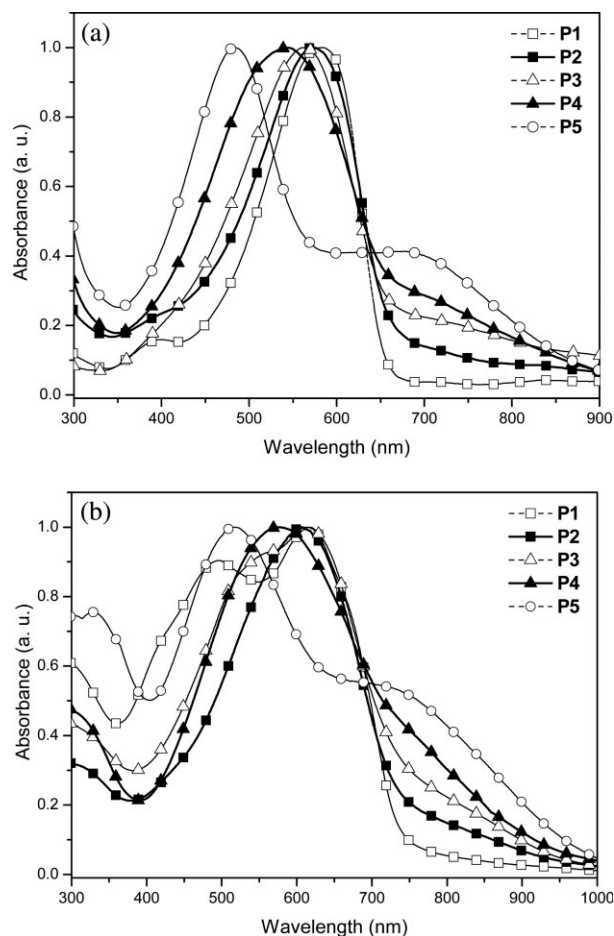
Figure 2. Normalized optical absorption spectra of D-A copolymers **P1–P5** in (a) solutions (in chloroform) and (b) solid films (spin-coating from chlorobenzene solutions).

peaks of **3** and **M2** at 312 nm[11(a)] and 513 nm, respectively, before copolymerization. The shorter wavelength absorption in the region of 350–550 nm (∼484 nm) resulted from the incorporated donor unit (**3**) in copolymer **P5**, which was hypsochromically shifted compared with the corresponding band of homopolymer **PCPDT** (λ_{max} = 565 nm). Besides, the longer wavelength absorption shoulder between 600 and 800 nm (ca. 705 nm) with tailing around 900 nm could be attributed to the acceptor unit (**M2**) incorporated with the main chain of copolymer **P5**, which agreed well with those observed in the CPDT polymer derivatives containing the acceptor unit (**M2**).[16] The main attribution of this effect can be explained by that the introduction of electron-deficient carbonyl moieties into the CPDT-based main-chain could also reduce the effective conjugation length of the polymer backbone, and thus, to induce a hypsochromic shift of the absorption spectrum. This phenomena is also suggestive by the *meta* conjugation effect observed from aminostilbenes[11(b)] and similar results with fluorene-CPDT-based copolymers.[11(c)] In other words, the electronic interaction between the carbonyl groups and the π-conjugated polymer backbones corresponds to the condition of *meta*-phenylene-bridged moieties.[11(c)] Therefore, copolymer **P5** exhibits a more blue-shifted absorption maximum (∼484 nm) than that of homopolymer **PCPDT** (∼565 nm) because of the *meta* conjugation effect to prevent the π-electron delocalization by carbonyl groups. Interestingly, reducing **M1** contents and increasing **M2** contents sequentially in copolymers **P2**, **P3**, and **P4**, gradual hypsochromic shifts of the short wavelength absorption

Table 2. Photophysical Data in Chloroform Solutions and Solid Films and Optical Band Gaps of Polymers **P1–P5**

| Polymer | λ_{max}, UV (nm) | | λ_{max}, PL (nm) | | $\Delta\lambda$ (nm)[a] | $E_{g,opt}$ (eV)[b] |
	Solution	Solid Film[c]	Solution	Solid Film		
P1	584	495, 620	653	724	36	1.70
P2	574	611	654	—[d]	37	1.59
P3	563 (704)[e]	609	654	—[d]	46	1.55
P4	544 (703)	582 (746)	—[d]	—[d]	38	1.73 (1.46)
P5	484 (705)	520 (750)	—[d]	—[d]	36	1.95 (1.38)

[a] $\Delta\lambda_{absorption} = \lambda_{max, film} - \lambda_{max, solution}$ (nm).
[b] Estimated from the onset wavelength of UV-vis spectra of the thin solid film.
[c] PL peaks were not detectable due to the PL quenching behavior.
[d] Spin-coated from chlorobenzene solution.
[e] Obtained from the wavelengths of shoulders (values in parentheses).

(∼560 nm) accompanying with slight increases of the longer shoulder absorption (∼700 nm) were observed in these copolymers. Hence, the introduction of electron-deficient carbonyl group in copolymer **P5** may reduce the effective conjugation length along the CPDT-based main chain because of the out of plane arrangements by the carbonyl groups of **M2**.

Figure 2(b) represents the UV-vis absorption spectra of solid films in the CPDT-based copolymers (**P1**–**P5**). The absorption spectra in solid films were generally similar to those in dilute solutions, where one maximum band in **P1** was centered at 620 nm and two characteristic bands in **P2**–**P5** were centered at 520–611 nm (for the shorter wavelength absorption) and 746–750 nm (for the longer wavelength shoulder absorption), respectively. Because of the interchain association and π-π stacking of these copolymers in solids, the maxima of the π-π* transitions generally had longer absorption maxima (36–46 nm of red shifts) in solid films than those in corresponding solutions. All copolymers (**P2**–**P5**) containing acceptor unit **M2** had broad absorption bands that extended to the near-infrared region with a maximum absorption shoulder λ_{max} at ∼750 nm, especially in **P5**. The long tailing around 900 nm in the absorption spectra of **P2**–**P5** could be observed in both solutions and solid films, which were attributed to their intrinsic properties rather than a reflection of poor film qualities. The optical band gaps ($E_{g,opt}$) of the copolymers in solid films, which were determined by the cutoff absorption wavelengths of the absorption spectra, are in the range of 1.38–1.70 eV (as shown in Table 2). As expected, the optical band gaps of all copolymers were not only much smaller than those of homopolymer **PCPDT**[13(b)] and copolymers of poly(3-alkylthiophene)s,[8(b),22] but also comparable with those of similar low band-gap copolymers, that is, poly(CPDT).[12,14(c),21(a)] Therefore, the idea of ICT interactions between electron donor and acceptor units in D-A copolymers is further supported by an efficient method to narrow down the band gaps of the conjugated polymers,[14(d),23] which suggests that these copolymers can be useful materials for future photovoltaic applications.

The PL spectra of copolymers **P1**–**P5** in chloroform solutions and solid films excited at incident wavelengths of 500 nm and 550 nm, respectively, are shown in Figure 3. The PL emission spectra of the CPDT-based copolymers in solutions were dramatically quenched, which were enhanced by increasing the contents of **M2** moieties in the D-A
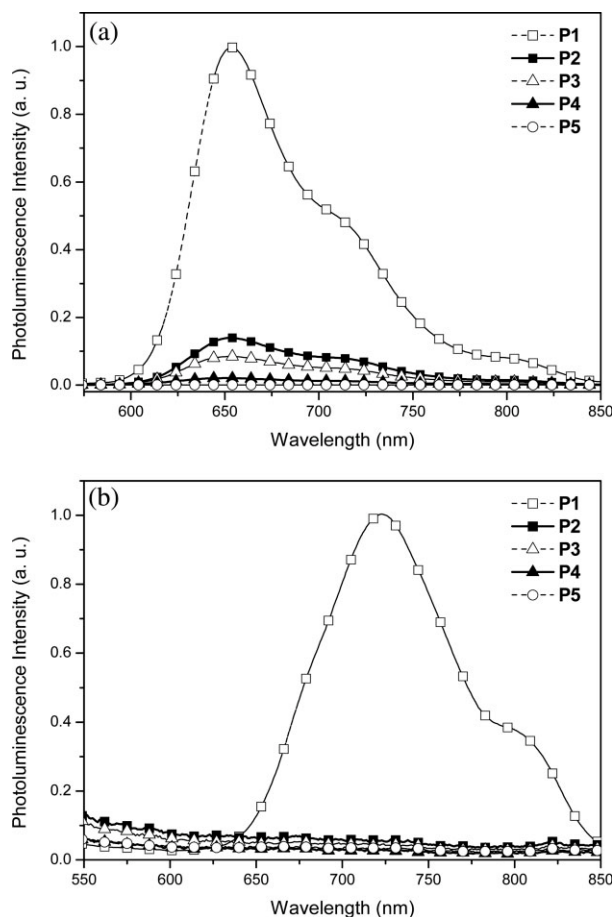

Figure 3. Normalized PL spectra of D-A copolymers **P1**–**P5** in (a) solutions (in chloroform) and (b) solid films (spin-coating from chlorobenzene solutions).

copolymers (**P1**–**P5**) as shown in Figure 3(a). Interestingly, the PL spectra of copolymers **P2**–**P5** containing **M2** moieties in Figure 3(b) were completely quenched in solid films. The PL quenching phenomena of these polymers might stem from the intersystem crossing from the photo-excited singlet state to the triplet one was induced by the carbonyl group, where intramolecular (in solution) and intermolecular (in film) energy transfer along the conjugated main chain occurs. Additionally, the red shift of PL spectra of **P1** from solution to film state might be due to the film morphology of highly crystallinity in **P1** as supported by XRD analysis, which will be described in the XRD section later. The corresponding optical properties of these copolymers in solid films, including the broad and strong optical absorptions, propose their potential applications in PVCs described below.

Electrochemical Characterization

The electronic states, that is, HOMO and LUMO levels, of the copolymers were investigated by CV to understand the charge injection processes in these new narrow-band-gap polymers and their PSC devices. The oxidation and reduction cyclic voltammograms of homopolymer **PCPDT** and copolymers **P1–P5** in solid films are displayed in Figure 4. To obtain solid films of an equal thickness, the concentration in the THF solutions and film forming conditions were kept constant ($\sim$5 mg/mL). The electrochemical measurements of the formal potentials, onset potentials, and band gaps, along with the estimated positions of the upper edges of the valence band (HOMO) and the lower edges of the conduction band (LUMO) are summarized in Table 3. As shown in Figure 4(a), the homopolymer **PCPDT** showed one reversible oxidation but no detectable reduction behavior, implying that the electrons are difficult to inject into this polymer. On the contrary, all copolymers **P1–P5** exhibited one reversible oxidation and two reversible or quasi-reversible reduction peaks as evident from the areas and close proximity of the anodic and cathodic scans in Figure 4(b), which are a good sign for high structural stability in the charged state. As illustrated in Table 3, the formal oxidation potentials of these polymers were in the range of 0.74–1.05 V, and their formal reduction potentials were in the ranges of -0.94 to -0.99 V and -1.16 to -1.95 V, respectively.

The moderate onset oxidation potentials and onset reduction potentials of copolymers **P1–P5** occurred between 0.5 and 0.85 V and about -0.81 V, respectively, from which the estimated HOMO levels of -4.90 to -5.25 eV and LUMO levels of about -3.59 eV were acquired according to the following equation:[19(b),24] $E_{\text{HOMO/LUMO}} = [-(E_{\text{onset}}$ (vs. Ag/AgCl)$-E_{\text{onset (Fc/Fc+ vs. Ag/AgCl)}}-4.8]$ eV, where 4.8 eV is the energy level of ferrocene below the vacuum level and $E_{\text{onset (Fc/Fc+ vs. Ag/AgCl)}} = 0.4$ eV. In addition, the onset oxidation potential of homopolymer **PCPDT** was observed at $\sim$0.55 V, from which the HOMO level of -4.95 eV was estimated. It is worthwhile to note that the HOMO energy levels of copolymers **P1–P5** were significantly varied relative to that of homopolymer **PCPDT** as measured under the same condition. Compared with **PCPDT**, the HOMO energy levels of copolymers **P4** to **P1** were reduced gradually by $\sim$0.1–0.3 eV via the incorporation of the increasing amounts of electron-withdrawing cyano groups into the polymer backbones. Therefore, based on the oxidation potential data, the
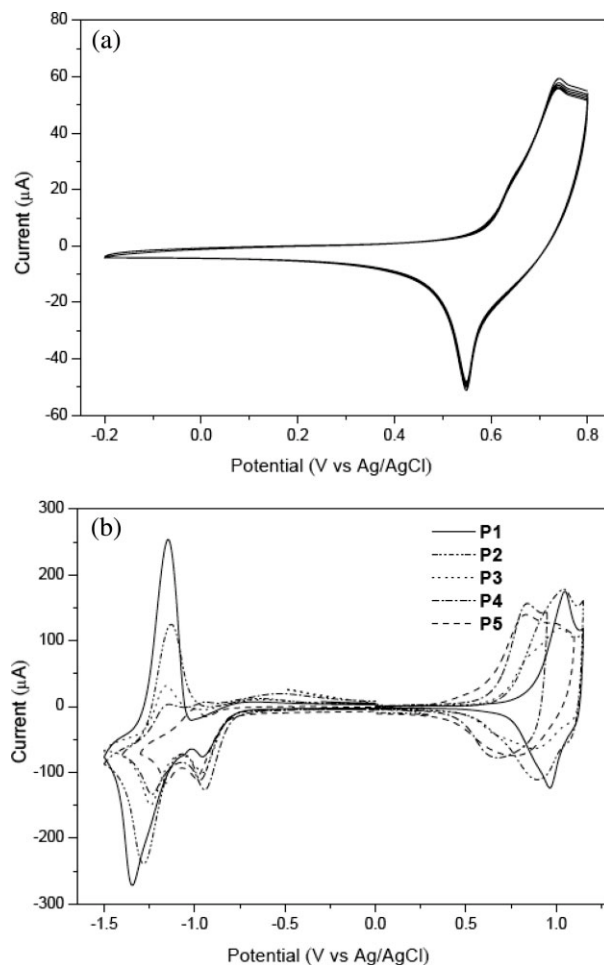

Figure 4. Cyclic voltammograms of (a) homopolymer **PCPDT** and (b) copolymers **P1–P5** (thin solid films) at a scan rate of 100 mV/s.

higher contents of electron-withdrawing cyano groups in copolymers **P1–P5** can induce the decreases in HOMO levels[17(a)] and show good air stabilities, especially for **P1**.[25] However, the HOMO energy level of copolymer **P5** was slightly higher than that of **PCPDT** (with a difference of $\sim$0.05 eV). It is probably that the electron-withdrawing effect of the ketone groups and the contribution of the primary resonance form might decrease the aromaticity of the system and hence to increase the quinoid character of the polymer backbones.[16(a),26] In contrast, the electrochemical reductions of copolymers **P1–P5** showed similar LUMO energy levels at about -3.59 to -3.60 eV, which represent to possess high electron affinities and also make these copolymers suitable donors for electron injection and transporting to PCBM acceptors (with 0.15–0.16 eV offsets in LUMO levels regarding PCBM with a LUMO level of -3.75

Table 3. Electrochemical Potentials, Energy Levels, and Band Gap Energies of Polymers **P1–P5**[a]

Polymer	Oxidation Potential V versus Ag/Ag$^+$		Reduction Potential V versus Ag/Ag$^+$		Energy Level[b] eV		Band Gap eV
	$E_{ox/onset}$[c]	$E_{ox/o}$[d]	$E_{red/onset}$[c]	$E_{red/o}$[d]	E_{HOMO}	E_{LUMO}	$E_{g,ec}$[e]
PCPDT	0.55	0.74	N. A[e]	N. A[e]	−4.95	N. A[e]	N. A[f]
P1	0.85	1.05	−0.81	−0.95	−5.25	−3.59	1.66
				−1.95			
P2	0.74	1.04	−0.81	−0.97	−5.14	−3.59	1.55
				−1.28			
P3	0.70	1.02	−0.81	−0.95	−5.10	−3.59	1.51
				−1.24			
P4	0.65	0.84	−0.81	−0.94	−5.05	−3.59	1.46
				−1.24			
P5	0.50	0.83	−0.80	−0.99	−4.90	−3.60	1.30
				−1.16			

[a] Reduction and oxidation potentials measured by cyclic voltammetry in solid films.
[b] Estimated from the onset potentials using empirical equations: $E_{HOMO}/E_{LUMO} = [-(E_{onset\ (vs.\ Ag/AgCl)} - E_{onset\ (Fc/Fc+\ vs.\ Ag/AgCl)}) - 4.8]$ eV where 4.8 eV is the energy level of ferrocene below the vacuum level and $E_{onset\ (Fc/Fc+\ vs.\ Ag/AgCl)} = 0.4$ eV.
[c] Onset oxidation and reduction potentials.
[d] Formal oxidation and reduction potentials.
[e] $E_{g,ec} = E_{ox/onset} - E_{red/onse}$.
[f] No properties of cathodic reduction potentials were available.

eV,[19] as shown in Fig. 5) for the polymeric BHJ solar cell devices.[27] Interestingly, the energy band gaps $E_{g,ec}$ ($E_{g,ec} = E_{ox/onset} - E_{red/onset}$, where $E_{g,ec}$ values are between 1.30 and 1.66 eV) measured directly from CV are close to the optical band gaps ($E_{g,opt}$ between 1.38 and 1.70 eV) acquired from the absorption spectra.

X-Ray Diffraction Analyses

To investigate the microstructural orders and molecular arrangements of thermal annealed CPDT-based copolymers in solids, XRD measurements were performed on powder samples before and after the thermal treatment at 150 °C. As shown in Figure 6, the annealed copolymers **P1** and **P5**
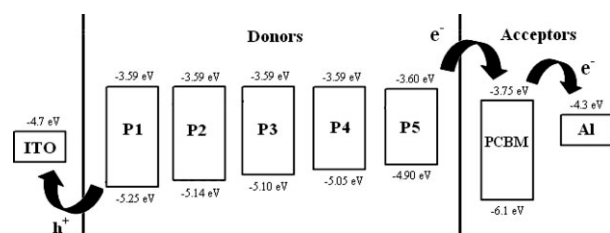
both exhibited well-crystalline patterns, which indicate highly ordered arrangements in solids. Distinct primary diffraction peaks, including one peak at $2\theta = 5.1°$ associated with a d-spacing value of 15.0 Å, were observed in copolymer **P1** after thermal annealing. Compared with **P1**, copolymer **P5** exhibited substantially a primary
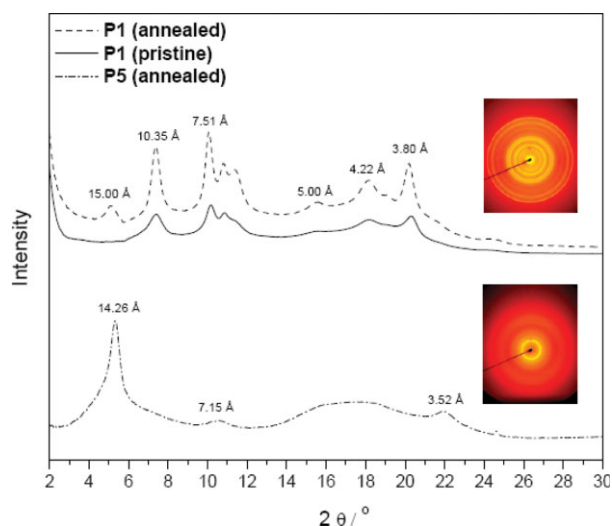

Figure 5. Energy band diagram with HOMO/LUMO levels of donor copolymers **P1–P5** and PCBM acceptor in relation to the work functions of ITO and Al (HOMO value of PCBM was from literature[19]).

Figure 6. Powder XRD patterns of copolymers **P1** (pristine and annealed samples) and **P5** (annealed sample). The sharp diffraction peaks indicated that the polymers formed an order structure in the solid state.

diffraction feature with a wider angle at $2\theta = 5.36°$ (corresponding to a smaller d-spacing value of 14.26 Å), which was assigned to a distance between the conjugated backbones separated by the long side chains as reported for other similar π-conjugated polymers with long pendants.[28] The XRD diffraction patterns at $2\theta = 10.2°$ and 10.7°, related to the d-spacing values of 7.51 and 7.15 Å for copolymers **P1** and **P5**, respectively, were the second-order peaks of the diffractions at 15.0 and 14.26 Å. Furthermore, copolymer **P1** showed a higher crystalline characteristic with a diffraction peak up to the third-order at $2\theta = 15.3°$, correlated to a d-spacing value of 5.0 Å. Because the effective cross section (S) of polymer pendent alkyl chains is equal to 20 Å, the hexagonal-like aggregations of the alkyl chains showed a characteristic side-to-side distance between alkyl chains with $d = 4.2$ Å.[29] The value observed for the diffraction feature at the d-spacing value of 4.22 Å in copolymer **P1** is in agreement with the result as previously reported.[29] However, the hexagonal-like aggregation about $d = 4.2$ Å was not observed in **P5**, which means that the alkyl side-chains in copolymer **P5** have less crystalline behavior (only amorphous halo observed $\sim 2\theta = 18°$) and the hexagonal-like aggregations of alkyl side-chains did not exist. Compared with copolymer **P1**, this lower packing order of the alkyl side-chains in **P5** might be due to the lower packing density of alkyl pendants from **M2** moieties in **P5** than that from **M1** moieties in **P1**. For the CPDT-based copolymers **P1** and **P5**, the diffraction features at $2\theta = 20.2°$ and 21.5°, corresponding to the d-spacing values of 3.80 and 3.52 Å, respectively, are close to the layer-to-layer π-π stacking distances between the coplanar backbones of the reported π-conjugated polymers[15(b),28–30] and being somewhat larger than the sheet-to-sheet distance of graphite (3.35 Å).[29(a)] The diffraction features of both copolymers **P1** and **P5** were often observed in the XRD patterns of the π-conjugated polymers.[15(b),28–30] On the basis of the observation, it can be assumed that copolymers **P1** and **P5** form good π-π stackings consisting of π-conjugated coplanar backbones, but **P1** has a better crystalline form in alkyl side chains than **P5**.

The possible packing motifs (side-view) of copolymers **P1** and **P5** are represented in Figure 7, which show a model that the alkyl side chains stack as bilayered packings and may have trivial interdigitated arrangements. It is interesting to note that the primary diffraction interchain distance of copolymer **P1** was somewhat (~ 0.74 Å)

larger than that of **P5** from XRD data. As possible side-view packing motifs in Figure 7, the cyanovinylene and phenylene segments in the polymer backbones of copolymer **P1** result in a more kinked molecular configuration with a wider π-π stacking region [5.59 E in Fig. 7(a)]. Comparatively, due to the only simple CPDT-based moieties in copolymer **P5**, the comparatively linear backbones of copolymer **P5** stack more compactly with a narrower rigid-core width [4.57 Å in Fig. 7(b)]. Since copolymers **P1** and **P5** have the same length of flexible tails, both copolymers might prefer the bilayered lamellar stacking in the soft regions with the same thickness of 5.2 Å $\times$ 2 = 10.4 Å. Therefore, the total lamellar thickness difference of 0.74 Å in the diffraction interchain distance of copolymers **P1** and **P5** from XRD data (15.0 and 14.26 Å for copolymers **P1** and **P5**, respectively) was induced from the variation of their backbones' widths in π-π stacking rigid-core regions, that is, $5.59 - 4.57 = 1.02$ Å, where 5.59 Å and 4.57 Å are the rigid-core regions of copolymers **P1** and **P5**, correspondingly. Moreover, the interchain lamellar d-spacing values of **P1** and **P5** (15.0 and 14.26 Å, respectively) from XRD are roughly equal to the total sum of the twice length of 2-ethylhexyl group plus the individual widths of their respective polymer backbones in the Chem3D ultra 8.0 calculations (~ 15.99 and 14.97 Å, correspondingly) from the side-view of Figure 7. This result suggests that the side chains of the copolymers likely stack as bilayered structures in the lamellar sheets, though the precise orientation of the alkyl side chains can not be determined with the present XRD information alone. The d-spacing values of 3.80 and 3.52 Å (obtained from XRD patterns at $2\theta = 20.2°$ and 21.5°) for copolymers **P1** and **P5** are correspondent to the (top-view) layer-to-layer π-π stacking distances between the top layer and bottom layer of the coplanar backbones in Figure 7(a,b), respectively. According to the XRD results, copolymer **P1** has more and sharper XRD peaks to possess a better crystallinity than **P5**, especially for wide angles of (top-view) alkyl side-chain arrangements, where the hexagonal-like aggregation (ca. $d = 4.2$ Å) was only observed in **P1**. Overall, the proposed model can explain the possible structural arrangements of the copolymer chains in copolymers **P1** and **P5**.

Polymeric Photovoltaic Cell Properties

The motivation for the design and syntheses of the conjugated CPDT-based copolymers is to look
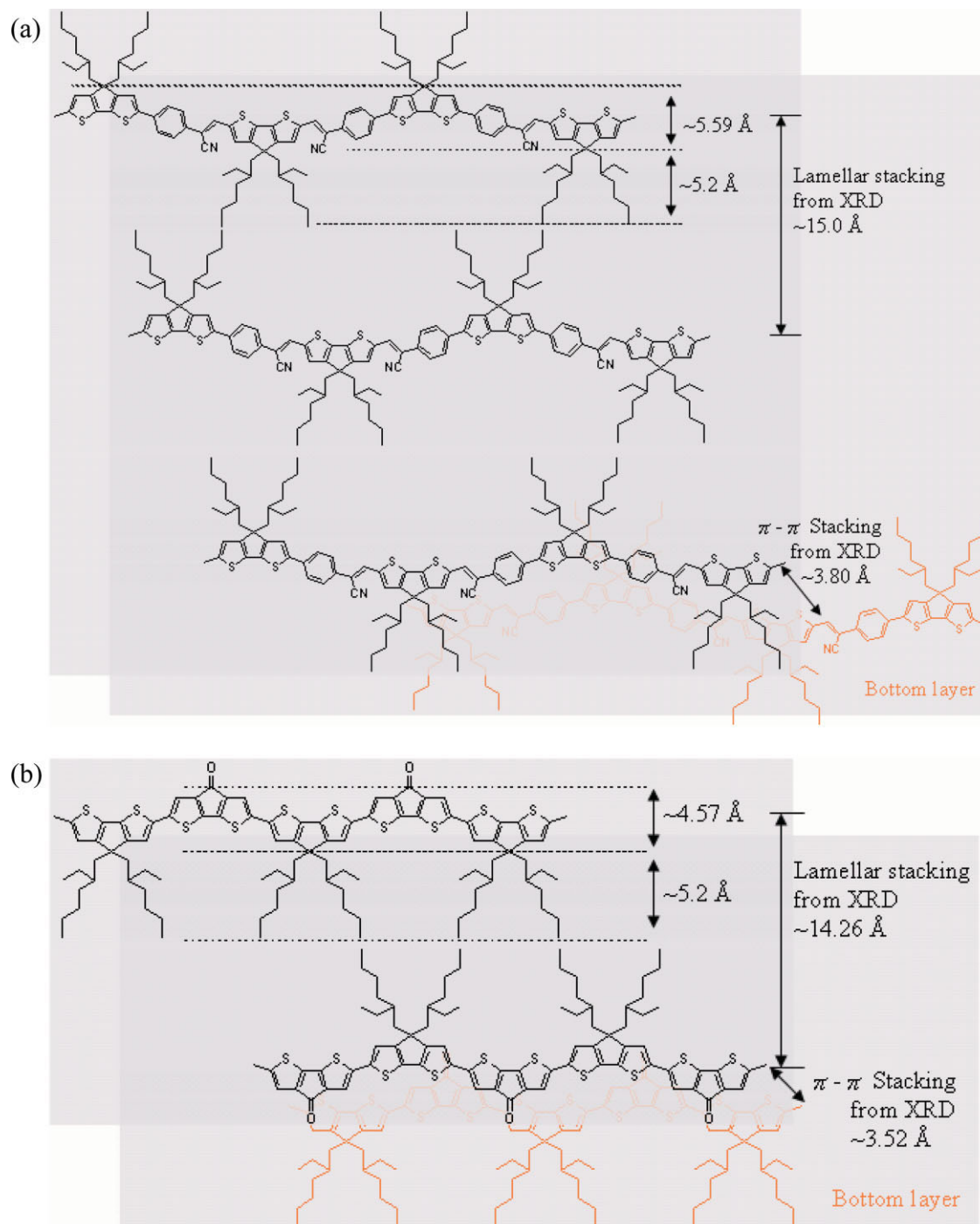
Figure 7. Schematic representation of a proposed layered and π-π stacked copolymer structure in the Chem3D ultra 8.0 calculations of (a) **P1** and (b) **P5** in solid state. [Color figure can be viewed in the online issue, which is available at www.interscience.wiley.com.]

for new narrow-band-gap polymers for the application of PSCs. To investigate the potential use of copolymers **P1**–**P5** in PSCs, BHJ devices were fabricated from an active layer in which copolymers **P1**–**P5** were blended with the complementary fullerene-based electron acceptor, PCBM, in a weight ratio of 1:4 (w/w). PSC devices with a configuration of ITO/PEDOT:PSS/**P1**–**P5**:PCBM

Table 4. Photovoltaic Properties of PSC Devices Containing an Active Layer of **P1–P5**:PCBM = 1:4 (w/w) with a Device Configuration of ITO/PEDOT:PSS/Polymer:PCBM/LiF/Al[a]

Active Layer[b] Polymer:PCBM	Thickness (nm)[b]	V_{oc} (V)	I_{sc} (mA/cm^2)	FF (%)	PCE (%)
P1	160	0.84	2.36	38	0.77
P2	140	0.48	0.77	23	0.08
P3	100	0.36	0.09	17	0.01
P4	140	0.49	0.67	25	0.08
P5	140	0.51	0.81	26	0.11

[a] Measured under AM 1.5 irradiation, 100 mW/cm^2.
[b] **P1–P5**:PCBM = with the fixed weight ratio of 1:4 (w/w).

(1:4 w/w)/LiF/Al were fabricated by depositing a thin layer (~50 nm) of PEDOT:PSS onto patterned ITO slides. The active layer (~100–160 nm) consisting of **P1–P5** and PCBM (1:4 w/w) was then deposited from a solution (10 mg/mL in chlorobenzene) by a spin rate of 800 rpm on the PEDOT:PSS film, and followed by the deposition of a LiF (~1 nm) and aluminum (120 nm) back electrode. The PSC devices were measured under AM 1.5 illumination for a calibrated solar simulator with an intensity of 100 mW/cm^2. The preliminarily obtained properties are summarized in Tables 4 and 5, and the typical *I–V* characteristics and EQE wavelength dependencies of all PSC devices are shown in Figure 8. Under the white-light illumination, the current density (I_{sc}), open circuit voltage (V_{oc}), and FF of the PSC devices composed of copolymers **P1–P5** were in the range of 0.09–2.36 mA/cm^2, 0.36–0.84 V, and 17–38%, respectively, with the PCE values between 0.01% and 0.77%.

The photovoltaic properties of the PSC devices containing CPDT-based copolymers **P1–P5** were dependent on the solubility and film-forming quality of the copolymers. Among these PSC devices containing **P1–P5**, copolymer **P1** gave the best performance in Figure 8(b) with I_{sc} = 2.36

mA/cm^2, V_{oc} = 0.84 V, FF = 38%, and PCE = 0.77%, respectively. Interestingly, the I_{sc} value of the PSC device containing **P1** was strongly enhanced relative to those containing **P2–P5** (by a factor of ~26 times higher than that of the worst **P3**), which might be due to the promoted solubility and the better film-forming capability by adding a higher molar ratio of **M1** units with alkyl side chains to **P1**. Ideally, the I_{sc} values were determined by the product of the photoinduced charge carrier densities and the charge carrier mobilities within the organic semiconductors.[10(b)] Thus, it can be recognized that the better results of I_{sc} and FF in the PSC device containing **P1** were obtained likely due to the well-balanced charge flow and less significant recombination loss[4(c),9(b)] originated from the highly ordered structural packing of alkyl side chains, as previously proved by the XRD patterns in the wide angle region of **P1**. However, the relatively low I_{sc} and FF values in the PSC device containing **P3** is poorly understood at this time, but it might be related to geminate charge recombination at the interface due to stable charge-transfer states, which limited the values of the photocurrents.[31(a)] Therefore, to further explore the dependence of charge transfer properties on the PSC devices, we

Table 5. Photovoltaic Properties[a] of Bulk-Heterojunction Solar Cells Containing an Active Layer of **P1**:PCBM = 1:4 (w/w) with Various Thicknesses

Thickness (nm)[b]	Spin Concentrations of Active Layer (**P1**:PCBM) (mg/mL:mg/mL)[c]	V_{oc} (V)	I_{sc} (mA/cm^2)	FF (%)	PCE (%)
120	5:20	0.77	0.42	15	0.05
160	10:40	0.84	2.36	38	0.77
310	20:80	0.83	1.46	25	0.31

[a] Measured under AM 1.5 irradiation, 100 mW/cm^2.
[b] The thickness (± 10 nm) was controlled by the solution concentrations of the active layer **P1**/PCBM (1:4 by wt.), and the spin rate of the active layer (**P1**/PCBM) was fixed at ca. 800 rpm.
[c] The active layer (**P1**/PCBM) was prepared from spin-coating of different solution concentrations (in chlorobenzene), but the weight ratio of **P1**:PCBM was fixed at 1:4.
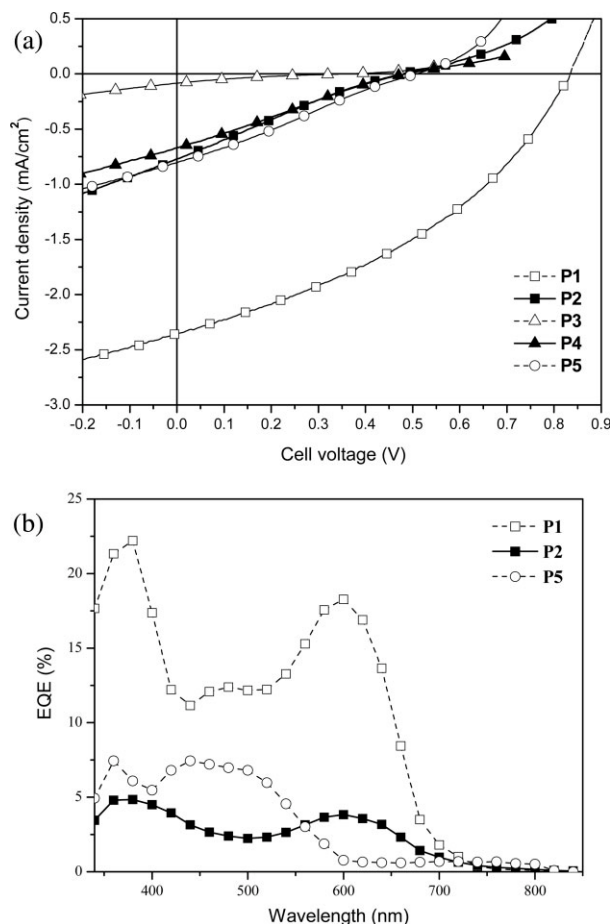
Figure 8. (a) *I–V* curves of solar cells with active layers **P1**–**P5**:PCBM (1:4 w/w) under simulated AM 1.5 solar irradiation. (b) EQE wavelength dependencies of solar cell devices based on active layers **P1**:PCBM, **P2**:PCBM, and **P5**:PCBM (1:4 w/w). Inset: representative device configuration.

have performed current measurements on hole-only and electron-only devices. The electron and hole mobilities can be determined precisely by fitting the plot of the current versus the voltage (*I–V*) curves for single carrier devices to the SCLC model.[31(b,c)] These devices in this study containing copolymers **P1**–**P5**:PCBM (1:4) blend film sandwiched between transparent ITO anode and cathode. The current is given by $J = 9\varepsilon_0\varepsilon_r\mu V^2/8L^3$, where $\varepsilon_0\varepsilon_r$ is the permittivity of the polymer, μ is the carrier mobility, L is the device thickness. The best result of hole mobility was found to be 9.74×10^{-6} cm^2/V/s for copolymer **P1**, and the others copolymers **P2**–**P5** were found to be below 1.41×10^{-6} cm^2/V/s. Reasonably, copolymer **P1** gave the best performance efficiency and highest photocurrent property in the PSC devices. Additionally, the electron mobilities of copolymers **P1**–**P5** were

found to be a range near $\sim4.78 \times 10^{-5}$ cm^2/V/s. In comparison with the hole- and electron-mobilities of these copolymers in the blend system (polymers:PCBM = 1:4), the electron-mobilities showed relatively fast charge transporting rates than that hole-mobilities because of larger PCBM amounts blended in the system. Therefore, it revels that the electron is the dominant charge carrier in the PSC devices, which results in the unbalanced charge transport obtained in this study.

The V_{oc} values were noticeably varied among the PSC devices containing copolymers **P1**–**P5**, which were related to the differences between the HOMO energy levels of the polymers and the LUMO energy levels of the acceptors.[10] Therefore, the HOMO energy levels of the donor polymers in PSC devices are very important to be finely tuned for PSC devices with high efficiencies. As discussed previously for the oxidation potentials of all copolymers, copolymer **P1** incorporated with the electron-withdrawing cyano groups has the lowest HOMO level among copolymers **P1**–**P5**. Thus, the highest V_{oc} value (0.84 V) is satisfactorily reached in **P1**, which has the highest V_{oc} value for any reported CPDT-based materials so far. Surprisingly, followed by the decrease of the HOMO levels (see Fig. 5), the V_{oc} values did not comply with the previous general regulation in the results of PSC devices for **P2**–**P5**. However, the photovoltaic parameters could be also influenced to some extent by the thickness of the active layer.[32] Especially for **P3**, although the copolymer had a medium HOMO level, its PSC device had the worst V_{oc} value owing to a worse film with a thinner thickness of about 100 nm induced by the poor solubility of copolymer **P3**.

To investigate the explanation for different efficiencies of the PSC devices, the EQE spectra of the PSC devices containing copolymers **P1**, **P2**, and **P5** blended with PCBM (1:4 w/w) as the photovoltaic layer are compared in Figure 8(b). The broad EQE curves of **P1**, **P2**, and **P5** covered almost the entire visible spectrum from 350 to 700 nm with maximum EQE values of 23%, 5%, and 8% for **P1**, **P2**, and **P5**, respectively. In a detailed comparison, the PSC devices containing **P1** and **P2** exhibited photovoltaic responses at both 380 and 600 nm, but with a shoulder at 470 nm only for **P1**. However, the PSC device containing **P5** merely showed the maximum EQE values at 360 and 440 nm, but the longer wavelength shoulder absorption of 700–750 nm (as shown in Fig. 2) was not observed in the EQE spectra. The
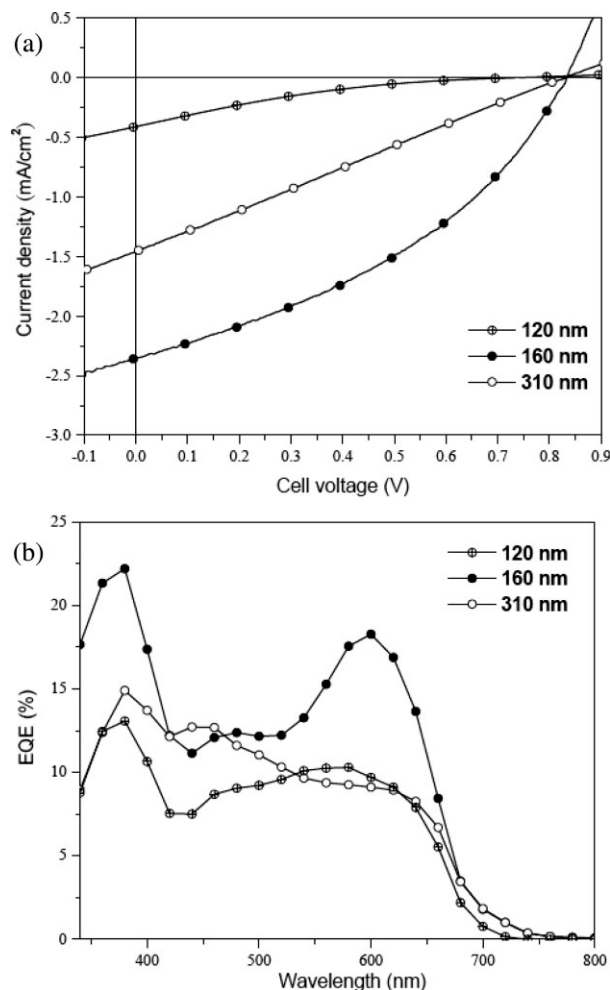
Figure 9. (a) *I–V* curves of solar cells under simulated AM 1.5 solar irradiation and (b) EQE spectra for PSC devices containing an active layer of **P1**:PCBM = 1:4 (w/w) with three different thicknesses (□) 120 nm, (●) 160 nm, and (○) 310 nm.

Finally, the effect of varying the thickness of the active layer on the photovoltaic performance of **P1**-based PSC devices is explored as shown in Figure 9 and Table 5. The thicknesses of the active layers were varied in the range of 120–310 nm by changing the spin concentrations (5, 10, and 20 mg/mL) of **P1** in chlorobenzene under the same spin rate. Quite surprisingly, decreasing the active layer thickness to 120 nm or increasing to 310 nm did not result in higher PCE efficiencies because there were simultaneous decreases in both FF and I_{sc} values as revealed in Figure 9(a). In contrast to the medium 160 nm thickness in the PSC device, both thicker (310 nm) and thinner (120 nm) devices showed slightly lower V_{oc} values but significantly reduced FF and I_{sc} values, where the thicker active layer had a combined influence on the hindered charge carrier transport or recombination[33] and the thinner active layer reduces the absorption of the irradiated light. As shown in Figure 9(b), a similar tendency was also conceived in EQE spectra, where the PSC device with the medium thickness of 160 nm possessed a maximal EQE of 23% at the irradiation wavelength of 350–400 nm. The higher EQE values covering the broad absorption wavelength region further explain the improved PSC performance of the medium thickness device (160 nm) over the other two devices with thicker and thinner thicknesses (310 nm and 120 nm). Additional improvements are underway to optimize the PSC devices by the modification of the film morphology, the process of thermal annealing treatments, and the replacement of some other electron acceptors, which can augment the formation of phase-separated structures and the charge mobilities.

CONCLUSIONS

Using the concept of incorporating electron-withdrawing groups in the D-A conjugated polymers, we have successfully synthesized five CPDT-based copolymers employing arylcyanovinyl and keto groups in different molar ratios by palladium(0)-catalyzed Suzuki coupling reactions. The band gaps and the HOMO/LUMO energy levels of these resulting copolymers can be finely tuned as demonstrated by the investigation of optical absorption properties and electrochemical studies. In powder XRD measurements, these copolymers exhibited obvious diffraction features indicating a highly ordered π-π stacking in the solid state. Preliminary PSC devices based on these five

result shows that the unit of monomer **M2** incorporated into the polymer backbone can not participate in the generation of photocurrents and thus to result in a feature of absorption limitation, which can be explained by the I_{sc} value of **P5** was relatively lower than that of **P1**. Comparing the PSC devices containing **P2** and **P5**, the measured current and EQE properties in the region of **P1** absorption comprised a wider wavelength range and a higher efficiency (with a maximal 4.6 times larger), which propose that **P1** somehow contributed significantly to the overall current generated by the (**P1**:PCBM)-based PSC device under illumination presumably owing to a more efficient intermolecular charge transfer.

copolymers blended with PCBM acceptors (1:4 w/w) had the PCE up to 0.77%, which gave the best performance with the values of $I_{sc} = 2.36$ mA/cm^2, FF = 38%, and $V_{oc} = 0.84$ V. Furthermore, this study provides novel conception that the HOMO energy levels can be reduced via the syntheses of merging with electron-withdrawing functional groups and thus the open-circuit voltage can be considerably enhanced, which will significantly improve the low V_{oc} values mainly possessed by most CPDT-based narrow-band-gap polymers.

REFERENCES AND NOTES

1. Yu, G.; Gao, J.; Hummelen, J. C.; Wudl, F.; Heeger, A. J. Science 1995, 270, 1789–1791.
2. (a) Thompson, B. C.; Fréchet, J. M. J. Angew Chem Int Ed 2008, 47, 58–77; (b) Kietzke, T.; Shin, R. Y. C.; Ayuk Mbi Egbe, D.; Chen, Z. K.; Sellinger, A. Macromolecules 2007, 40, 4424–4428; (c) Uhrich, C.; Schueppel, R.; Petrich, A.; Pfeiffer, M.; Leo, K.; Brier, E.; Kilickiran, P.; Baeuerle, P. Adv Funct Mater 2007, 17, 2991–2999.
3. (a) Bouclé, J.; Ravirajanac, P.; Nelson, J. J Mater Chem 2007, 17, 3141–3153; (b) Beek, W. J. E.; Wienk, M. M.; Janssen, R. A. J. Adv Funct Mater 2006, 16, 1112–1116; (c) Moet, D. J. D.; Koster, L. J. A.; de Boer, B.; Blom, P. W. M. Chem Mater 2007, 19, 5856–5861; (d) Beek, W. J. E.; Wienk, M. M.; Janssen, R. A. J. Adv Mater 2004, 16, 1009–1013.
4. (a) Li, G.; Shrotriya, V.; Huang, J.; Yao, Y.; Moriarty, T.; Emery, K.; Yang, Y. Nat Mater 2005, 4, 864–868; (b) Koppe, M.; Scharber, M.; Brabec, C.; Duffy, W.; Heeney, M.; McCulloch, I. Adv Funct Mater 2007, 17, 1371–1376; (c) Ma, W.; Yang, C.; Gong, X.; Lee, K.; Heeger, A. J. Adv Funct Mater 2005, 15, 1617–1622.
5. (a) Coffey, D. C.; Reid, O. G.; Rodovsky, D. B.; Bartholomew, G. P.; Ginger, D. S. Nano Lett 2007, 7, 738–744; (b) Wienk, M. M.; Wiljan, J. M. K.; Verhees, J. H.; Knol, J.; Hummelen, J. C.; Hal, P. A. v.; Janssen, R. A. J. Angew Chem Int Ed 2003, 42, 3371–3375.
6. (a) Alstrup, J.; Norrman, K.; Jorgensen, M.; Krebs, F. C. Sol Energy Mater 2006, 90, 2777–2792; (b) Chabinyc, M. L.; Street, R. A.; Northrup, J. E. Appl Phys Lett 2007, 90, 123508–123513.
7. (a) Gadisa, A.; Mammo, W.; Andersson, L. M.; Admassie, S.; Zhang, F.; Andersson, M. R.; Inganäs, O. Adv Funct Mater 2007, 17, 3836–3842; (b) Ashraf, R. S.; Hoppe, H.; Shahid, M.; Gobsch, G.; Sensfuss, S.; Klemm, E. J Polym Sci Part A: Polym Chem 2006, 44, 6952–6961; (c) Li, K. C.; Hsu, Y. C.; Lin, J. T.; Yang, C. C.; Wei, K. W.; Lin, H. C. J Polym Sci Part A: Polym Chem 2008, 46, 4285–4304; (d) Lee, J.; Jung, B. J.; Lee, S. K.; Lee, J. I.; Cho, H. J.; Shim, H. K. J Polym Sci Part A: Polym Chem 2005, 43, 1845–1857; (e) Tsami, A.; Yang, X. H.; Farrell, T.; Neher, D.; Holder, E. J Polym Sci Part A: Polym Chem 2008, 46, 7794–7808.
8. (a) Tang, W. H.; Kietzke, T.; Vemulamada, P.; Chen, Z. K. J Polym Sci Part A: Polym Chem 2007, 45, 5266–5276; (b) Zhao, C. C.; Chen, X. H.; Zhang, Y.; Ng, M. K. J Polym Sci Part A: Polym Chem 2008, 46, 2680–2688; (c) Ayuk Mbi Egbe, D.; Nguyen, L. H.; Schmidtke, K.; Wild, A.; Sieber, C.; Guenes, S.; Sariciftci, N. S. J Polym Sci Part A: Polym Chem 2007, 45, 1619–1631; (d) Cheng, K. F.; Chueh, C. C.; Lin, C. H.; Chen, W. C. J Polym Sci Part A: Polym Chem 2008, 46, 6305–6316; (e) Ouhib, F.; Dkhissi, A.; Iratçabal, P.; Hiorns, R. C.; Khoukh, A.; Desbrières, J.; Pouchan, C.; Dagron-Lartigau, C. J Polym Sci Part A: Polym Chem 2008, 46, 7505–7516.
9. (a) Xia, P. F.; Lu, J. P.; Kwok, C. H.; Fukutani, H.; Wong, M. S.; Tao, Y. J Polym Sci Part A: Polym Chem 2009, 47, 137–148; (b) Huo, L.; Tan, Z.; Wang, X.; Zhou, Y.; Han, M. F.; Li, Y. F. J Polym Sci Part A: Polym Chem 2008, 46, 4038–4049; (c) Huo, L.; He, H.; Han, M. F.; Zhou, E.; Li, Y. F. J Polym Sci Part A: Polym Chem 2007, 45, 3861–3871.
10. (a) Scharber, M. C.; Mühlbacher, D.; Koppe, M.; Denk, P.; Waldauf, C.; Heeger, A. J.; Brabec, C. J. Adv Mater 2006, 18, 789–794; (b) Günes, S.; Neugebauer, H.; Sariciftci, N. S. Chem Rev 2007, 107, 1324–1338; (c) Brabec, C. J.; Cravino, A.; Meissner, D.; Sariciftci, N. S.; Fromherz, T.; Rispens, M. T.; Sanchez, L.; Hummelen, J. C. Adv Funct Mater 2001, 11, 374–380.
11. (a) Coppo, P.; Turner, M. L. J Mater Chem 2005, 15, 1123–1133; (b) Yang, J. S.; Liau, K. L.; Tu, C. W.; Hwang, C. Y. J. Phys Chem A 2005, 109, 6450–6456; (c) Pal, B.; Yen, W. C.; Yang, J. S.; Chao, C. Y.; Hung, Y. C.; Lin, S. T.; Chuang, C. H.; Chen, C. W.; Su, W. F. Macromolecules 2008, 41, 6664–6671.
12. (a) Kraak, A.; Wieserma, A. K.; Jordens, P.; Wynberg, H. Tetrahedron 1968, 24, 3381–3398; (b) Berlin, A.; Brenna, E.; Pagani, G. A.; Sannicolo,

F. Synth Met 1992, 51, 287–297; (c) Cunningham, D. D.; Gaa, A.; Pham, C. V.; Lewis, E. T.; Burkhardt, A.; Davidson, L. L.; Kansah, A. N.; Ataman, O. Y.; Zimmer, H.; Mark, H. B. J Electrochem Soc 1988, 135, 2750.

13. (a) Zotti, G.; Schiavon, G. Macromolecules 1994, 27, 1938–1942; (b) Asawapirom, U.; Scherf, U. Macromol Rapid Commun 2001, 22, 746–749; (c) Coppo, P.; Cupertino, D. C.; Yeates, S. G.; Turner, M. L. Macromolecules 2003, 36, 2705–2711; (d) Cremer, L. D.; Vandeleene, S.; Maesen, M.; Verbiest, T.; Koeckelberghs, G. Macromolecules 2008, 41, 591–598.

14. (a) Lee, J. K.; Ma, W. L.; Brabec, C. J.; Yuen, J.; Moon, J. S.; Kim, J. Y.; Lee, K.; Bazan, G. C.; Heeger, A. J. J Am Chem Soc 2008, 130, 3619–3623; (b) Peet, J.; Kim, J. Y.; Coates, N. E.; Ma, W. L.; Moses, D.; Heeger, A. J.; Bazan, G. C. Nat Mater 2007, 6, 497–500; (c) Mü1hlbacher, D.; Scharber, M.; Morana, M.; Zhu, Z.; Waller, D.; Gaudiana, R.; Brabec, C. Adv Mater 2006, 18, 2884–2889; (d) Zhu, Z.; Waller, D.; Gaudiana, R.; Morana, M.; Mü1hlbacher, D.; Scharber, M.; Brabec, C. Macromolecules 2007, 40, 1981–1986; (e) Moulé, A. J.; Tsami, A.; Bünnagel, T. W.; Forster, M.; Kronenberg, N. M.; Scharber, M.; Koppe, M.; Morana, M.; Brabec, C. J.; Meerholz, K.; Scherf, U. Chem Mater 2008, 20, 4045–4050; (f) Xiao, S.; Zhou, H.; You, W. Macromolecules 2008, 41, 5688–5696.

15. (a) Zhan, X.; Tan, Z.; Domercq, B.; An, Z.; Zhang, X.; Barlow, S.; Li, Y.; Zhu, D.; Kippelen, B.; Marder, S. R. J Am Chem Soc 2007, 129, 7246–7247; (b) Zhang, M.; Tsao, H. N.; Pisula, W.; Yang, C.; Mishra, A. K.; Müllen, K. J Am Chem Soc 2007, 129, 3472–3473.

16. (a) Lambert, T. L.; Ferraris, J. P. J Chem Soc Chem Commun 1991, 752; (b) Ferraris, J. P.; Lambert, T. L. J Chem Soc Chem Commun 1991, 1268; (c) Berlin, A.; Zotti, G.; Zecchin, S.; Schiavon, G.; Vercelli, B.; Zanelli, A. Chem Mater 2004, 16, 3667–3676.

17. (a) Roncali, J. Macromo Rapid Commun 2007, 28, 1761–1775; (b) van Mullekom, H. A. M.; Vekemans, J. A. J. M.; Havinga, E. E.; Meijer, E. W. Mater Sci Eng 2001, 32, 1–40.

18. (a) Lucas, P.; El Mehdi, N.; Anh Ho, H.; Belanger, D.; Breau, L. Synthesis 2000, 9, 1253–1258; (b) Brzezinski, J. Z.; Reynolds, J. R. Synthesis 2002, 8, 1053–1056.

19. (a) Brabec, C. J.; Sariciftci, N. S.; Hummelen, J. C. Adv Funct Mater 2001, 11, 15–26; (b) Al-Ibrahima, M.; Rotha, H. K.; Zhokhavetsb, U. Solar Energy Mater Solar Cells 2005, 85, 13–20.

20. (a) Wu, C. W.; Tsai, C. M.; Lin, H. C. Macromolecules 2006, 39, 4298–4305; (b) Wu, C. W.; Lin, H. C. Macromolecules 2006, 39, 7232–7240.

21. (a) Liao, L.; Dai, L.; Smith, A.; Durstock, M.; Lu, J.; Ding, J.; Tao, Y. Macromolecules 2007, 40, 9406–9412; (b) Zhu, Y.; Champion, R. D.; Jenekhe, S. A. Macromolecules 2006, 39, 8712–8719.

22. (a) Osaka, I.; Sauvé, G.; Zhang, R.; Kowalewski, T.; McCullough, R. D. Adv Mater 2007, 19, 4160–4165; (b) Hou, J.; Tan, Z.; Yan, Y.; He, Y.; Yang, C.; Li, Y. J Am Chem Soc 2006, 128, 4911–4916.

23. (a) Hou, Y.; Chen, Y.; Liu, Q.; Yang, M.; Wan, X.; Yin, S.; Yu, A. Macromolecules 2008, 41, 3114–3119; (b) Colladet, K.; Fourier, S.; Cleij, T. J.; Lutsen, L.; Gelan, J.; Vanderzande, D. Macromolecules 2007, 40, 65–72.

24. Shahid, M.; Ashraf, R. S.; Klemm, E.; Sensfuss, S. Macromolecules 2006, 39, 7844–7853.

25. Leeuw, D. M.; Simenon, M. M. J.; Brown, A. R.; Einhard, R. E. F. Synth Met 1997, 87, 53–59.

26. (a) Roncali, J. J Mater Chem 1999, 9, 1875; (b) Roncali, J. Chem Rev 1997, 97, 173–206.

27. Mihailetchi, V. D.; Duren, J. K. J.; Blom, P. W. M.; Hummelen, J. C.; Janssen, R. A. J.; Kroon, J. M.; Rispens, M. T.; Verhees, W. J. H.; Wienk, M. M. Adv Funct Mater 2003, 13, 43–46.

28. (a) Lu, G.; Usta, H.; Risko, C.; Wang, L.; Facchetti, A.; Ratner, M. A.; Marks, T. J. J Am Chem Soc 2008, 130, 7670–7685; (b) Yasuda, T.; Sakai, Y.; Aramaki, S.; Yamamoto, T. Chem Mater 2005, 17, 6060–6068.

29. (a) Yamamoto, T.; Arai, M.; Kokubo, H.; Sasaki, S. Macromolecules 2003, 36, 7986–7993.

30. (a) Cao, J.; Kampf, J. W.; Curtis, M. D. Chem Mater 2003, 15, 404–411; (b) Yamamoto, Y.; Lee, B. L. Macromolecules 2002, 35, 2993–2999; (c) Ong, B. S.; Wu, Y. L.; Liu, P.; Gardner, S. J Am Chem Soc 2004, 126, 3378–3379; (d) Morana, M.; Wegscheider, M.; Bonanni, A.; Kopidakis, N.; Shaheen, S.; Scharber, M.; Zhu, Z.; Waller, D.; Gaudiana, R.; Brabec, C. Adv Funct Mater 2008, 18, 1757–1766.

31. (a) Morteani, A. C.; Sreearunothai, P.; Herz, L. M.; Friend, R. H.; Silva, C. Phys Rev Lett 2004, 92, 247402–247404; (b) Blom, P. W. M.; deJong, M. J. M.; vanMunster, M. G. Phys Rev B 1997, 55, R656; (c) Dunlap, D. H.; Parris, P. E.; Kenkre, V. M. Phys Rev Lett 1996, 77, 542–545.

32. Moulé, A. J.; Bonekamp, J. B.; Meerholz, K. J Appl Phys 2006, 100, 094503–094507.

33. (a) Markov, D. E.; Hummelen, J. C.; Blom, P. W.; Sieval, A. B. Phys Rev B 2005, 72, 045216–045225; (b) Kietzke, T.; Horhold, H.; Neher, D. Chem Mater 2005, 17, 6532–6537.